

Relational representation in the olfactory system

Thomas A. Cleland*, Brett A. Johnson†, Michael Leon†‡, and Christiane Linster*

*Department of Neurobiology and Behavior, Cornell University, Ithaca, NY 14853; and †Department of Neurobiology and Behavior, University of California, Irvine, CA 92697

Edited by Linda M. Bartoshuk, University of Florida, Gainesville, FL, and approved December 13, 2006 (received for review October 4, 2006)

The perceptual quality of odors usually is robust to variability in concentration. However, maps of neural activation across the olfactory bulb glomerular layer are not stable in this respect; rather, glomerular odor representations both broaden and intensify as odorant concentrations are increased. The relative levels of activation among glomeruli, in contrast, remain relatively stable across concentrations, suggesting that the representation of odor quality may rely on these relational activity patterns. However, the neural normalization mechanisms enabling extraction of such relational representations are unclear. Using glomerular imaging activity profiles from the rat olfactory bulb together with computational modeling, we here show that (i) global normalization preserves concentration-independent odor-quality information; (ii) perceptual similarities, as assessed behaviorally, are better predicted by normalized than by raw bulbar activity profiles; and (iii) a recurrent excitatory circuit recently described in the olfactory bulb is capable of performing such normalization. We show that global feed-forward normalization in a sensory system is behaviorally relevant, and that a center-surround neural architecture does not necessarily imply center-surround function.

coding | computational neuroscience | glomerulus | mitral cell | short-axon cell

The accurate, replicable perception of stimulus quality over a wide range of intensities is a central issue in sensory neuroscience. Fundamental limitations in the physics of sampling and unpredictable sources of interference generate variance in primary sensory maps that subsequent processing layers must deconstruct to synthesize a useful stimulus representation. Indeed, percepts of stimulus quality generally are synthetic, arising from directed compilations of sensory information. For example, visual stimuli are represented in unpredictable coordinates on the retina, with the visual percept of an object ultimately being synthesized from numerous sequential primary images. The timbre of a clarinet, the stationary component of which largely is derived from the ratios of amplitudes of the overtones of a fundamental frequency, can be identified irrespective of the pitch or volume of a given note. Features of texture can be identified across a range of absolute pressures. In each of these cases, information necessary to identify critical features of stimulus quality must be contained in the relative, or relational, response profiles of activated sensory channels, rather than their absolute activity levels.

Relational representations depend on the broad patterns of primary sensory activation that typically are observed in response to elemental stimuli. For example, the movement of a single vibrissa evokes responses across a broad region of somatosensory cortex (1), a single point of light evokes widespread activity in visual cortex (2), and a single pure tone elicits a response across large areas of auditory cortex (3). Odorants evoke comparably broad responses in the mammalian olfactory system. Primary olfactory sensory neurons (OSNs) express a single olfactory receptor (OR) species in rodents, yet are broadly selective for odorant stimuli (4–6), such that even monomolecular odorants can evoke responses across much of the epithelium (7) and the glomerular layer of the olfactory bulb (OB) (8). Because of the convergence of OSNs expressing the same OR species onto common glomeruli, the pattern of activated glo-

meruli on the surface of the OB reflects the pattern of activated ORs, thus clearly identifying the constellation of chemical qualities that constitute the presented odor (8–11).

We investigated the possibility that relational representations enable the maintenance of odor quality over large differences in odorant concentration and the mechanism by which the olfactory system can maintain these relational representations. It has been well established that the degree of overlap among different glomerular activity maps reflects odorant structural commonalities and corresponds to the perceptual similarity of odors (12–15). However, this relationship breaks down when odorant concentration is included as a variable. OSN activation profiles and the corresponding glomerular activity maps universally become broader and more intense when odors are presented at higher concentrations (Fig. 1A) (16–20), simply because higher odorant concentrations recruit additional OSN populations with progressively lower affinities for the presented agonist(s).

Normalization of glomerular activity maps mitigates these disruptive effects of concentration. In contrast to absolute maps of glomerular activity, normalized glomerular images reveal odor-specific maps that are substantially insensitive to concentration (Fig. 1B) (17, 21). By implication, this normalized output would be mediated by mitral cells, second-order principal neurons that integrate inputs from primary sensory neurons and interneurons within the OB.

The computation of intensity-independent stimulus representations in sensory systems depends on the existence of associated inhibitory systems that are activated more broadly by sensory stimuli than are the principal neurons receiving direct sensory inputs (22–24). Specifically, inhibition that is uniformly distributed across the input field, perhaps representing an average or sum of all input activity, will tend to preserve the pattern of relative activation levels across the field irrespective of total intensity, whereas inhibition that is delivered in proportion to local activation levels, or in an otherwise biased manner, will retain concentration-dependent distortions in the resulting output patterns. Recent work in the OB (25, 26) has identified an interconnected network of excitatory juxtglomerular interneurons, external tufted (ET) and short-axon (SA) cells, that delivers inhibition onto OB principal neurons (mitral cells) via local inhibitory neurons [periglomerular (PG) cells], and it has been suggested that this recurrent excitatory network mediates the uniform inhibition required for concentration-invariant secondary representations and other odor-processing mechanisms (22). We show here that this interglomerular excitatory network, via activation of local inhibitory neurons and with estimates of synaptic densities and connectivity derived from experimental

Author contributions: T.A.C., B.A.J., M.L., and C.L. designed research, performed research, analyzed data, and wrote the paper.

The authors declare no conflict of interest.

This article is a PNAS direct submission.

Abbreviations: OSN, olfactory sensory neuron; OB, olfactory bulb; OR, olfactory receptor; ET, external tufted; SA, short-axon; PG, periglomerular; Hn, habituation trial *n*.

‡To whom correspondence should be addressed. E-mail: mleon@uci.edu.

This article contains supporting information online at www.pnas.org/cgi/content/full/0608564104/DC1.

© 2007 by The National Academy of Sciences of the USA

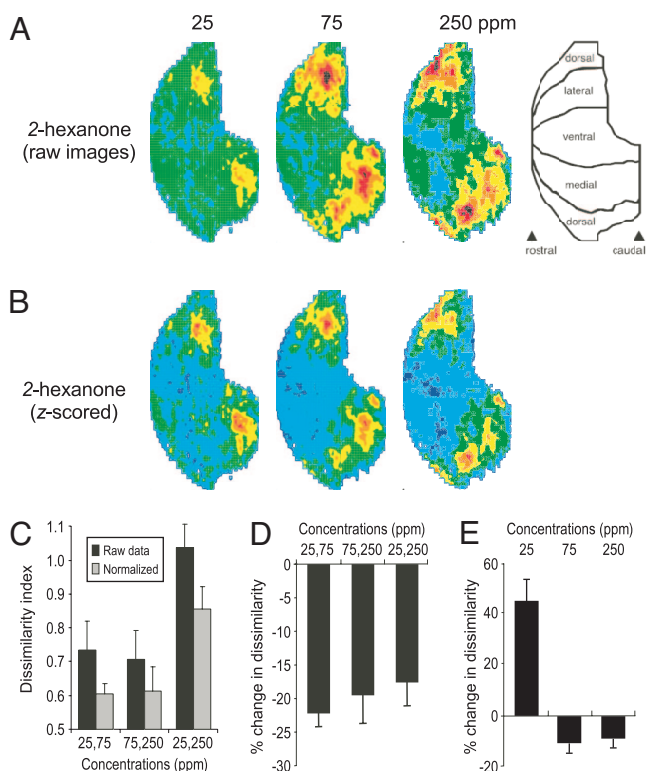


Fig. 1. Normalization of OB odor-response patterns. (A) Raw glomerular activity maps in response to presentation of 2-hexanone at three vapor-phase concentrations. (B) A z score normalization of these activity maps results in a representation that depends less on concentration. (C) Combined data from four odorants (2-hexanone, methyl valerate, *n*-pentanal, and *n*-pentanol) illustrating the reduction in pattern dissimilarity across concentrations produced by normalization. Dissimilarity indices between glomerular activity maps of the same odorant presented at different concentrations were reduced for all pairs of concentrations and all odorants tested after z score normalization. (D) The proportional reduction in pattern dissimilarity across all pairs of concentrations and odorants. (E) Proportional changes in pattern dissimilarity between odorant pairs presented at the same concentration, averaged across all pairwise comparisons.

data, is not only capable of computing the required normalization but also seems optimized to perform this operation. Using a full-scale, 2,200-glomerulus model to process and analyze 2-deoxyglucose imaging data from the rat OB, along with behavioral data, we demonstrate the feasibility and potential mechanism of perceptual concentration invariance in olfaction.

Results

Because normalization is effected at the level of mitral cells, which often are inhibited below baseline by odorant presentation, we normalized with respect to the mean by using a z score transformation [$z_i = (x_i - \mu_x)/\sigma_x$]. To measure the similarity between glomerular activation patterns, we calculated pairwise indices of dissimilarity (normalized Euclidean distance) between the raw and normalized patterns of activation evoked by four odorants (2-hexanone, methyl valerate, *n*-pentanal, and *n*-pentanol) at vapor-phase concentrations of 25, 75, and 250 ppm. The indices of dissimilarity between the normalized patterns evoked by any given odorant across concentrations were reduced significantly as compared with those of the corresponding raw patterns ($P < 0.05$ in all cases; Fig. 1 C and D), indicating that normalized patterns represent concentration-invariant quality information significantly better than do raw response patterns. In contrast, dissimilarity indices between pairs of different odorants at the same concentration were not reduced consis-

tently by normalization; effects varied from a marginal reduction to a substantial increase in dissimilarity (Fig. 1E).

If normalized glomerular activity patterns represent the output of bulbar computations performed on raw input patterns, then they should be better predictors of perceptual similarity than the raw patterns. Indeed, quantitative comparisons between glomerular activation patterns and olfactory perception generally have been based on normalized data (12–14, 27, 28). To test this hypothesis, we selected odorant pairs in which the raw glomerular patterns evoked by the two odorants at a given concentration are more similar to one another than are those evoked by different concentrations of the same odorant (Fig. 2A). In contrast, when the activity patterns of these odorants are normalized, the representations of each odorant are more similar to one another, irrespective of concentration, than they are to those evoked by the other odorant at any concentration (Fig. 2B). We tested which of these predictions of perceptual similarity was supported by behavioral data by using a spontaneous, nonassociative odor-discrimination test (12–14). Briefly, we first habituated rats to the presentation of one odorant of each pair (2-hexanone or *n*-pentanal) at 25 ppm and then measured their novelty responses to presentation of (i) the same odorant at 75 ppm and (ii) the paired odorant (methyl valerate or *n*-pentanol, respectively) at 25 ppm (Fig. 2C). The results show that rats perceive the two concentrations of either odorant as more similar to one another than to the different odorant (Fig. 2D), demonstrating that normalized glomerular representations predict perceptual similarity whereas raw patterns do not.

Normalization by the Interglomerular Network. Normalized glomerular response profiles better represent intensity-independent quality information and are superior predictors of odor perception than the corresponding raw activation patterns are. We asked where in the olfactory sensory network such normalization might be performed. Raw glomerular activation patterns correspond largely to the activity of convergent OSNs, increasing in intensity and breadth with higher odorant concentrations (16–20). Mitral cells receive afferent input directly from OSNs; however, they do not as a rule demonstrate monotonic increases in spike rate when presented with higher odorant concentrations nor do they exhibit broadening of their receptive fields (29–33). Hence, normalization in some form takes place within the OB, and its computation presumably depends on the heterogeneous network of juxtglomerular interneurons that, along with direct afferent stimulation, regulates mitral cell activity.

We constructed a detailed, full-scale, 2,200-glomerulus model of the glomerular layer of the OB to study how normalization could be computed. OSNs and PG, ET, SA, and mitral cells were represented and synaptically connected as described experimentally (Fig. 3A) (25, 26, 34). Briefly, each population of OSNs converging on a given glomerulus was represented by a single aggregate OSN; hence, the model contained 2,200 such OSNs. For any given odor, the activation level of each OSN was drawn from a corresponding data point collected in 2-deoxyglucose imaging experiments, enabling the model to be presented with receptor activation profiles corresponding to those evoked by real odorant stimuli (absent any temporal component). Within each glomerulus, OSNs synaptically excited PG, ET, and mitral cells, whereas PG cells in turn directly inhibited mitral cells. ET cells excited both PG cells associated with the same glomerulus and SA cells within a 2-glomerulus radius (25, 26). SA cells did not receive monosynaptic input from OSNs but were activated by ET cells; they in turn excited ET and PG cells in several neighboring glomeruli. Importantly, the mutual excitation between ET and SA neurons constituted a recurrent excitatory network extending laterally across the glomerular layer, the output of which was delivered to PG cells and, subsequently, to mitral cells as inhibition (26). The strength, density, and physical

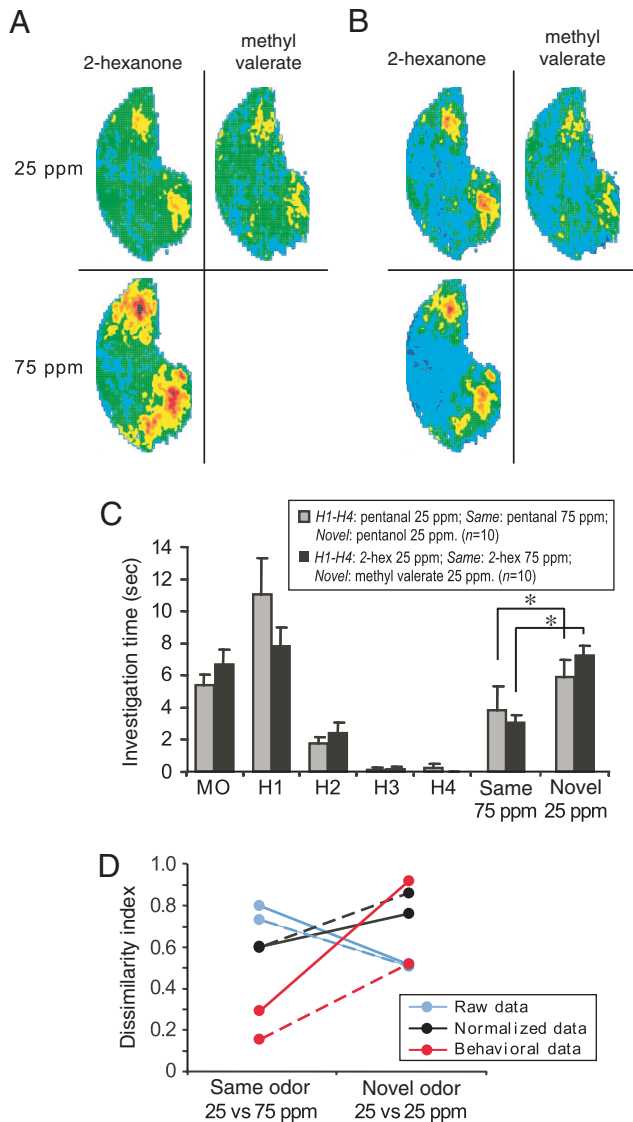


Fig. 2. Relationship between glomerular activity maps and perceptual responses. (A) Raw glomerular activity maps evoked by 2-hexanone (25 and 75 ppm) and methyl valerate (25 ppm) predict that 2-hexanone presented at 25 ppm should be perceived as more similar to methyl valerate (at 25 ppm) than to itself at 75 ppm. (B) In contrast, z score-normalized glomerular activity maps predict that 2-hexanone will be perceived as more similar to itself, irrespective of concentration, than to methyl valerate. (C) Results from a cross-habituation study demonstrate that these odorants are more perceptually similar to themselves across concentrations than they are to other odorants. After a baseline presentation of mineral oil solvent (MO) followed by four presentations of the habituating stimulus (*n*-pentanal or 2-hexanone at 25 ppm; H1–H4), rats responded to presentation of a novel odorant at 25 ppm (*n*-pentanal or methyl valerate, respectively) with a significantly greater novelty response than they did to presentation of the habituation odorant at a higher concentration (75 ppm; *, $P < 0.01$ in both cases). (D) For both odor pairs, perceptual dissimilarity (red) covaried with the dissimilarity in normalized (black) and not raw (blue) glomerular activity maps. Solid lines, 2-hexanone vs. methyl valerate; dashed lines, *n*-pentanal vs. *n*-pentanal.

distribution of these recurrent connections among glomeruli were variables of interest (Fig. 3B).

We used the model to transform input profiles derived from nonnormalized 2-deoxyglucose images of odor-specific activation patterns in the OB (glomerular activity) (35) into mitral cell response profiles, which were averaged over the time of stimulus application and depicted as activity maps (mitral cell activity).

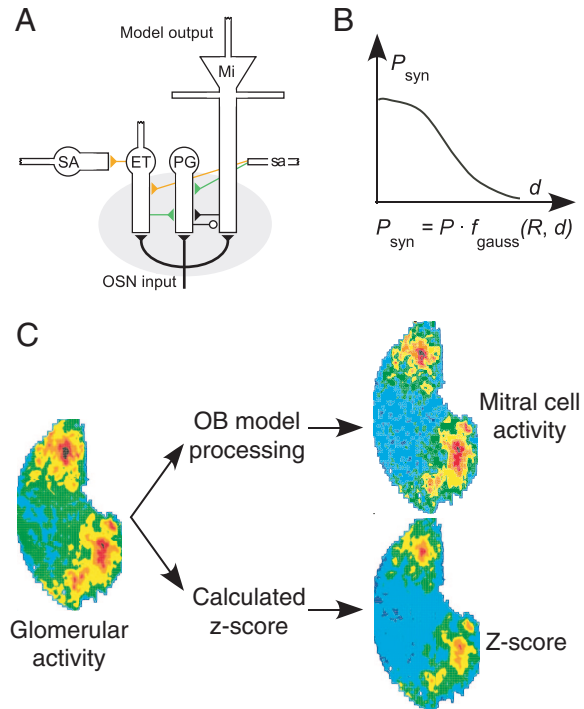


Fig. 3. Glomerular layer circuitry and model architecture. (A) Schematic of the glomerular layer network. Triangles connote excitatory synapses; open circles indicate inhibitory synapses. OSN input is delivered onto mitral cells (Mi), ET cells, and a minority of PG cells. ET cells activate SA cells, and these two cell types form a recurrent excitatory network (red synapses). The output of this network is delivered to PG cells (blue synapses), which in turn inhibit mitral cells. (B) Illustration of the spatial distribution of ET/SA network projections in the model. To match experimental estimates of ET/SA connectivity (26), the probability of synaptic formation between a given SA cell and a distant target cell (P_{syn}) was the product of a baseline probability $P = 0.1$ and a Gaussian distribution $f_{gauss}(R, d)$ that declined with the distance d between the two cells. The breadth of the distribution of projection distances was determined by the standard breadth R . Experimental estimates were best matched by radius $R = 2$ glomerular diameters for inputs to SA cells and a radius of $R = 7$ glomerular diameters for SA outputs. (C) Raw glomerular activity maps were derived directly from patterns of 2-deoxyglucose uptake in the rat OB. Calculated normalization of these data by using a z score statistic yielded normalized activity maps that were less sensitive to concentration differences and more predictive of perceptual similarities. The raw glomerular activity maps also were processed by the OB model, in which patterns of mitral cell output activity reflect the normalizing effect of the recurrent excitatory network. The output patterns of mitral cell activity are compared directly with calculated z score normalizations.

These simulated output maps then were compared with calculated z score normalizations of the same data (8) to measure how well the model network computed this normalization (Fig. 3C) and to what extent this operation depended on particular network parameters.

Optimization of Local Inhibitory Synaptic Strength. Normalization with respect to the mean requires subtraction of the average input strength from the representations of individual stimulus features. Hence, the network must both compute an estimate of this average input strength and scale this average appropriately for delivery onto mitral cells as inhibition. We tested the sufficiency of the interglomerular network to meet this criterion. Presentation of an odorant stimulus to the model evoked a characteristic pattern of activation among OSNs (Fig. 4*Ai*). OSN activity in turn excited ET, SA, and PG interneurons (directly or indirectly) as well as mitral cells. Critically, lateral excitatory projections mediated by ET/SA cells acted to reduce the variance

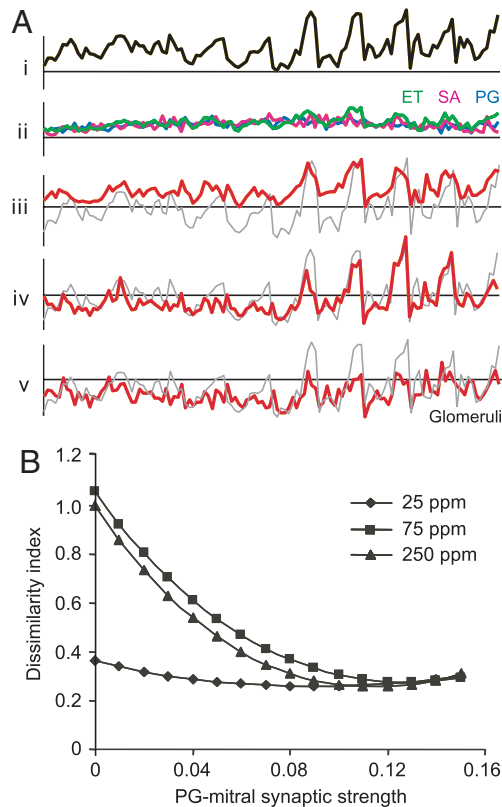


Fig. 4. Optimization of the strength of PG inhibition of mitral cells. (A) Activity across a selected 120-glomerulus region of the rat OB in response to the presentation of 2-hexanone. Glomeruli are depicted along the abscissa in arbitrary order; ordinate values represent the activity of selected cell types. Horizontal lines depict baseline activity levels in the absence of odor. (i) Activity profile of OSN inputs (raw glomerular activation). (ii) Resulting activity profiles of ET, SA, and PG cells. (iii) In the absence of PG cell inhibitory input to mitral cells, the activity profile of the mitral cell population (red trace) directly reflects that of the incoming OSNs. The gray trace depicts the calculated z score of OSN activity. (iv) The mitral cell activity profile (red trace) when PG-to-mitral synaptic strength is optimal resembles that of the calculated z score (gray trace). (v) Overly strong inhibition of mitral cells results in broad suppression of mitral cell activity (red trace). (B) Plot of the dissimilarity index (Euclidean distance) between 2-hexanone activity patterns derived from full-scale (2,200-glomerulus) model output and the calculated normalization of the same input data as a function of PG-mitral synaptic weight. Notably, the dissimilarity index is minimal at approximately the same synaptic weight (0.11 arbitrary units) irrespective of stimulus concentration.

in activation levels among the interneurons associated with different glomeruli (Fig. 4*Aii*).

In the absence of inhibitory inputs from PG cells, mitral cell response profiles directly reflected the raw patterns of OSN activation. With PG-mediated inhibition active, however, mitral cell responses were modulated by the interglomerular network (Fig. 4*Aiii-v*). The effects of a range of inhibitory synaptic weights were simulated, and the results were assessed by measuring the normalized Euclidean distance between model output and the calculated z score normalization of the same glomerular input data. A common synaptic weight was found to be optimal for approximating a z score normalization irrespective of odorant or concentration (Fig. 4*B*).

Optimization of Lateral Excitatory Network Properties. The SA cell is the main contributor to interglomerular connectivity (26). Interglomerular projections from SA interneurons radiate in all directions from the soma. The density of these processes declines with distance, indicating a center-surround topological organi-

zation. Specifically, based on retrograde dye transport from focal injections into individual glomeruli, it has been estimated that half of the interneurons projecting to a given glomerulus are located at distances within 5–7 glomerular diameters ($\approx 350 \mu\text{m}$) of the injection site, whereas only 10% are located at distances farther than 15–18 glomerular diameters ($\approx 850 \mu\text{m}$). Functional imaging has shown that the lateral spread of excitation from focal glomerular stimulation extends up to $900 \pm 93 \mu\text{m}$ from the stimulus site, covering nearly the entirety of the visible OB. The functional effect of this lateral excitatory network on mitral cells is inhibitory; stimulation of interglomerular connections abruptly ($6.5 \pm 1.2\text{-ms}$ latency) terminates long-lasting depolarizations in mitral cells located $150\text{--}525 \mu\text{m}$ away and reduces the amplitudes of newly generated long-lasting depolarizations via a GABA_Aergic mechanism (26).

The ability of this interglomerular network to mediate the uniform global inhibition of mitral cells relies critically on the connectivity of the ET/SA recurrent excitatory network. Recurrent excitatory networks, if activity is bounded or balanced so as to avoid runaway positive feedback, have the property of equalizing the level of activity among interconnected neurons. Consequently, if the lateral projections of SA cells and their mutually excitatory synapses with ET and other SA cells are sufficiently extensive to approximate a fully connected network, then their inhibition of mitral cells via PG cells, in principle, would be uniform across the entire glomerular layer, reflecting the average activity of all OSNs. We asked whether experimental estimates of ET/SA lateral connectivity among glomeruli could support this operation.

Initial parameters in the model were set to replicate experimental estimates of ET/SA connectivity. Each SA cell had a baseline $P = 0.1$ probability to synapse on ET, SA, and PG cells in other glomeruli, modulated as a function of distance d along the trajectory of a Gaussian distribution [$f_{\text{gauss}}(R, d)$] with a standard deviation R of 7 glomerular diameters (Fig. 3*B*). These parameters generated appropriate connectivity maps in which $\approx 50\%$ of all connections to a given cell originated from SA cells located within 5–7 glomerular diameters and 10% originated from SA cells located 15–18 glomeruli away. The strength of the PG-to-mitral inhibitory synapse was set to its optimum (Fig. 4*B*). We then varied the baseline synaptic probability (P) and projection distance (R) parameters of the ET/SA network systematically in the model. Increases in either of these parameter values increased the average number of synapses that each cell received from SA cells [SA synaptic density; Fig. 5*A*; also see supporting information (SI) Fig. 6]. To ensure that only the distribution, and not the overall strength, of the interglomerular excitatory network was varied, individual synaptic weights were reduced as synaptic probabilities, and projection distances were increased so that the average total weight of excitatory synapses received by a given cell type was held constant. The SA synaptic density thereby directly reflected the level of interglomerular connectivity. The standard deviation of SA cell activity across the glomerular layer was large in the absence of lateral connectivity, reflecting the diverse odor-activation levels of different glomeruli, but converged rapidly toward an asymptotic minimum when the average SA synaptic density exceeded roughly four SA synapses per postsynaptic neuron (Fig. 5*B*) irrespective of stimulus concentration (SI Fig. 7). The model output more closely approximated a z score transformation of input activity as ET/SA activity became more uniform across the glomerular layer (Fig. 5*C*). Critically, the experimentally estimated values for interglomerular connectivity correspond precisely with the minimum level of connectivity required to achieve asymptotically uniform global feed-forward inhibition (Fig. 5*B* and SI Fig. 7, dashed vertical lines). This finding has two major implications. First, it suggests an optimization for uniform global inhibition because the minimum synaptic density necessary to achieve this effect

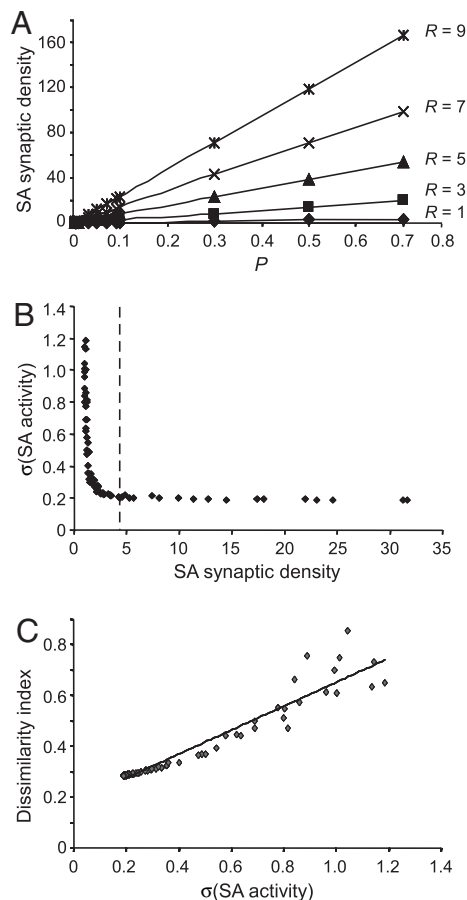


Fig. 5. Effects of the probability and spatial distribution of SA output connections. (A) Effect of separately varying the probability of synaptic connections (P) and the radius of their distribution (R) of connection probabilities (Fig. 3B) on the number of synapses received from SA neurons by any given cell (SA synaptic density). (B) SA synaptic density determined the regional variability in SA activation levels across the network (standard deviation of SA activity), reaching an asymptotic minimum at approximately four inputs per glomerulus independent of stimulus concentration. Experimental estimates of ET/SA connectivity (26) (dashed lines) correspond to the minimum degree of synaptic connectivity that can effectively achieve uniform feed-forward inhibition and compute a global normalization. Data shown are for a concentration of 75 ppm; similar results were observed at other concentrations (SI Fig. 7). (C) The quality of the normalization performed by the glomerular network (compared with a calculated z score) depends quasi-linearly on the uniformity of the computation of the mean across the ET/SA recurrent excitatory network. Indices of dissimilarity between model output and calculated z score normalizations of afferent data were directly proportional to the standard deviation of activity levels across this interglomerular network.

appears to have been deployed in the OB. Second, it demonstrates that a center-surround projection architecture, such as that exhibited by SA neurons (26), does not necessarily imply center-surround functionality.

Discussion

The simulations presented here demonstrate the feasibility and mechanism of stimulus normalization in olfaction and support a unique computational role for the recurrent excitatory network recently described in the OB glomerular layer. In concert with related glomerular processing circuitry (22, 36), this mechanism enables functional interpretation of observations that odors commonly evoke inhibitory responses in mitral cells and that increasing odorant concentrations do not monotonically increase spike rates in mitral cells (29), setting the stage for

subsequent processing by the mitral–granule cell network (35, 37). Moreover, behavioral assays confirm that normalized olfactory representations predict perceptual relationships across concentrations, whereas raw glomerular representations do not.

The OB recurrent excitatory network, comprising ET and SA neurons, is activated by odor presentation that excites ET cells along with mitral cells and a minority of PG cells (25, 26). The spread of excitation through the ET/SA network equalizes the activity of these cells across the glomerular layer at a level corresponding to the total input strength. Importantly, although the lateral projections of SA interneurons are distributed more densely among neighboring than among distant glomeruli, demonstrating a type of center-surround architecture in the glomerular layer (26), our results show that this localized architecture does not necessarily imply center-surround functionality. Rather, the recurrent excitatory network generates a spatially uniform level of activity across the glomerular layer, perhaps corresponding to the broad, diffuse activity observed in intrinsic imaging studies of the OB (18). Moreover, these results suggest that this network deploys the minimum number of synaptic connections and the narrowest distribution of projection distances sufficient to produce such uniform activity. The net effect of this global feed-forward inhibition is to reduce significantly the impact of stimulus concentration on the activity level of the secondary olfactory representation, constructing a relational odor representation at the level of mitral cells that enables the perceptual constancy of odor quality across the ranges of concentrations inevitably encountered in natural environments.

Materials and Methods

Activation Maps. Odorant exposures for mapping 2-deoxyglucose uptake in rat OB were performed as described previously (17, 38). Glomerular layer uptake was mapped into data matrices that were standardized in dimensions relative to anatomical landmarks. Activation patterns were calculated by converting grayscale levels obtained from the digitized images into units of nanocuries per gram (nCi/g; 1 Ci = 37 GBq) of tissue through comparison to radioactivity standards exposed on the same films.

A z score-normalized counterpart for each raw glomerular activation map was calculated by subtracting the mean value of all data points from each data point and then dividing each difference by the standard deviation of all data points, resulting in a transformed data set with a mean of zero and a standard deviation of unity. Raw and normalized glomerular activation maps, as well as model output maps, corresponding to four different odorants presented at three different concentrations (see SI Table 1) were compared by calculating the normalized Euclidean distances between all possible pairs of maps.

Perceptual Comparisons. We measured the perceptual similarity of odor pairs in rats ($n = 10$) by using a cross-habituation test (12, 13). Odorants were dissolved in mineral oil and presented by pipetting 60 μ l of the odor stimulus onto a filter paper disk in a weighing dish that was placed on top of the wire cage cover. Test sessions consisted of one 50-sec presentation of vehicle followed by four 50-sec presentations of the habituation odorant at 5-min intervals and, finally, one 50-sec presentation of the test odorant. The time that the rat spent investigating the odorant (active sniffing within 1 cm) during each trial was recorded. Perceptual dissimilarity indices were calculated as the root-mean-square of the differences between investigation times during the final habituation trial (H4) and the test trial, normalized by the root-mean-square of the differences between H4 and the initial presentation of the habituation odorant (H1; Fig. 2C).

Computational Modeling. Our OB model (27) includes five neuron types: OSNs and PG, ET, SA, and mitral cells (Fig. 3A). Because

these simulations were concerned exclusively with computations in the glomerular layer, granule cells and mitral cell lateral dendrites were omitted. All neurons were represented as single compartments, each characterized by a membrane time constant that can be regarded as the mean product of the membrane capacitance and input resistance. Odor inputs to the simulations were drawn directly from raw 2-deoxyglucose activity maps of the OB glomerular layer; i.e., real primary odorant representations were used as input.

The model simulated interactions among the major cell types described in the glomerular layer (Fig. 3A), with estimates of interglomerular connectivity derived from the literature (26). Synapses received from OSNs as well as those between PG and mitral cells were local to each glomerulus, whereas synapses received from SA cells, as well as those from ET to SA cells, were

drawn from different glomeruli as a probabilistic function of interglomerular distance (Fig. 3B). For each pair of interacting cells, the probability of a synaptic connection was computed according to a probability density function defined by a baseline probability of connection and the breadth of the distribution of possible interactions (Fig. 3B). These distributions were modeled as Gaussian with a standard deviation equal to the breadth term R and a peak scaled to the baseline probability P of synaptic interactions. Modeling equations can be found in *SI Text*, and parameters are outlined in *SI Table 2*.

We thank C. Kiselycznyk for behavioral experiments. This work was supported by National Institute on Deafness and Other Communication Disorders Grants DC005727 and DC007725 (to T.A.C.) and DC003545 and DC006516 (to M.L.).

1. Brett-Green BA, Chen-Bee CH, Frostig RD (2001) *J Neurosci* 21:9944–9954.
2. Grinvald A, Lieke EE, Frostig RD, Hildesheim R (1994) *J Neurosci* 14:2545–2568.
3. Bakin JS, Kwon MC, Masino SA, Weinberger NM, Frostig RD (1996) *Cereb Cortex* 6:120–130.
4. Duchamp-Viret P, Chaput MA, Duchamp A (1999) *Science* 284:2171–2174.
5. Katada S, Hirokawa T, Oka Y, Suwa M, Touhara K (2005) *J Neurosci* 25:1806–1815.
6. Araneda RC, Kini AD, Firestein S (2000) *Nat Neurosci* 3:1248–1255.
7. Araneda RC, Peterlin Z, Zhang X, Chesler A, Firestein S (2004) *J Physiol* 555:743–756.
8. Johnson BA, Farahbod H, Xu Z, Saber S, Leon M (2004) *J Comp Neurol* 480:234–249.
9. Leon M, Johnson BA (2003) *Brain Res Brain Res Rev* 42:23–32.
10. Wachowiak M, Denk W, Friedrich RW (2004) *Proc Natl Acad Sci USA* 101:9097–9102.
11. Friedrich RW, Korsching SI (1997) *Neuron* 18:737–752.
12. Cleland TA, Morse A, Yue EL, Linster C (2002) *Behav Neurosci* 116:222–231.
13. Linster C, Johnson BA, Yue E, Morse A, Xu Z, Hingco EE, Choi Y, Choi M, Messiha A, Leon M (2001) *J Neurosci* 21:9837–9843.
14. Linster C, Johnson BA, Morse A, Yue E, Leon M (2002) *J Neurosci* 22:6842–6845.
15. Youngentob SL, Johnson BA, Leon M, Sheeche PR, Kent PF (2006) *Behav Neurosci* 120:1337–1345.
16. Guthrie KM, Gall CM (1995) *Chem Senses* 20:271–282.
17. Johnson BA, Leon M (2000) *J Comp Neurol* 422:496–509.
18. Meister M, Bonhoeffer T (2001) *J Neurosci* 21:1351–1360.
19. Wachowiak M, Cohen LB (2001) *Neuron* 32:723–735.
20. Stewart WB, Kauer JS, Shepherd GM (1979) *J Comp Neurol* 185:715–734.
21. Wachowiak M, Cohen LB, Zochowski MR (2002) *J Neurophysiol* 87:1035–1045.
22. Cleland TA, Sethupathy P (2006) *BMC Neurosci* 7:7.
23. Lauritzen TZ, Miller KD (2003) *J Neurosci* 23:10201–10213.
24. Troyer TW, Krukowski AE, Miller KD (2002) *J Neurophysiol* 87:2741–2752.
25. Hayar A, Karnup S, Ennis M, Shipley MT (2004) *J Neurosci* 24:6676–6685.
26. Aungst JL, Heyward PM, Puche AC, Karnup SV, Hayar A, Szabo G, Shipley MT (2003) *Nature* 426:623–629.
27. Linster C, Cleland TA (2004) *J Comput Neurosci* 16:39–47.
28. Guerrieri F, Schubert M, Sandoz JC, Giurfa M (2005) *PLoS Biol* 3:e60.
29. Chalansonnet M, Chaput MA (1998) *Chem Senses* 23:1–9.
30. Wellis DP, Scott JW, Harrison TA (1989) *J Neurophysiol* 61:1161–1177.
31. Hamilton KA, Kauer JS (1989) *J Neurophysiol* 62:609–625.
32. Harrison TA, Scott JW (1986) *J Neurophysiol* 56:1571–1589.
33. Meredith M (1986) *J Neurophysiol* 56:572–597.
34. Shipley MT, Ennis M (1996) *J Neurobiol* 30:123–176.
35. Cleland TA, Linster C (2005) *Chem Senses* 30:801–813.
36. Rubin DB, Cleland TA (2006) *J Neurophysiol* 96:555–568.
37. Kay LM, Stopfer M (2006) *Semin Cell Dev Biol* 17:433–442.
38. Johnson BA, Woo CC, Hingco EE, Pham KL, Leon M (1999) *J Comp Neurol* 409:529–548.